EASR

Engineering and Applied Science Research

https://www.tci-thaijo.org/index.php/easr/index

Published by the Faculty of Engineering, Khon Kaen University, Thailand

# Designing a feedback breathable soft-stuffed robot: Exploring its potential for enhancing sleep quality

Kanjanapan Sukvichai*, Tanapon Kitmuti and Kan Yajai

Department of Electrical Engineering, Faculty of Engineering, Kasetsart University, Bangkok 10900, Thailand

Received 11 October 2023
Revised 1 March 2024
Accepted 7 March 2024

**Abstract**

Insomnia significantly impacts human productivity and can lead to long-term health issues. Sleeplessness is often caused by stress, particularly in adults. While hugging another human or animal can effectively reduce stress due to the breathing motion synchronization, but it is often challenging and impractical in many situations. This study proposes a potential alternative solution to alleviate stress by utilizing a soft-stuffed robot. The robot is designed with a breathing mechanism that mimics the respiration of a living being. By using flexible 3D materials, artificial ribs and spine are created to imitate animal breathing motion. The 3D materials are carefully selected due to their properties. To measure the human breathing rhythm, a biosensor called Medtex, consisting of conductive fabric, can captures the human signal. This signal is then utilized as feedback in a control system, employing a PID control algorithm to achieve synchronization between the robot and human breathing motion in terms of phase and frequency. The robot imitator actuator, a customized Maxon RE motor, is controlled by a magnetic encoder and feedback signal. To ensure safety and comfort, the imitator is enveloped in a cushion. Experimental trials conducted during nighttime involved volunteers hugging the robot while sleeping, with the resulting output recorded and analyzed. The findings demonstrate that the designed robot can be effectively controlled and accurately determine sleep states with proper synchronization.

**Keywords:** Breathable soft-stuffed robot, Respiration imitator, Flexible 3D printable material, Conductive fabric

## 1. Introduction

Insomnia, a common sleep disorder affecting a significant portion of the population, has detrimental effects on daytime productivity and overall well-being. It is particularly prevalent among adults and can lead to various health issues, including a weakened immune system [1]. However, improving sleep quality is a complex challenge [2]. Stress is a major contributor to sleep disturbances, and studies have shown that interactions with pets can help alleviate stress [3-5]. Unfortunately, owning and caring for real animals may not be feasible for individuals living in urban areas due to restrictions or time constraints. In such cases, a soft-stuffed robot with an animal-like appearance can serve as a viable alternative to provide comfort and stress relief, although it cannot fully replace the experience of interacting with a real animal. The breathing pattern of an animal robot differs significantly from that of a real animal because of the limited degrees of freedom. To enhance the sense of realism and comfort, it is important for the robot to have a simulated breathing mechanism. In a previous study [6], researchers explored the potential of a biofeedback therapeutic animal robot. A soft-stuffed robot can be effectively utilized for various human-related purposes, such as promoting wellness, addressing medical needs, and supporting psychological well-being.

Previous studies have provided evidence of the positive health benefits associated with human-companion animal interactions [3-6]. However, utilizing real animals for therapeutic purposes can be impractical and pose complications such as mismatched life cycles, unexpected habits, allergies, or illness risks. To overcome these challenges, the use of friendly-looking robots emerges as a more suitable solution. These animal-like dolls or robots, designed to mimic the physical characteristics of real animals using mechanics and electronics components, offer practicality and applicability in real-world scenarios. The effectiveness of such mechanisms in providing companionship has been demonstrated by credible evidence in the field of companion robot usage [6, 7]. Additionally, the exploration of breathing animal toys has shown promising results in improving infant respiration.

This research aimed to address stress-induced sleeplessness by utilizing a robot-based approach. The study focused on activating the autonomic nervous system through external breathing stimuli as an effective treatment for stress-induced sleeplessness in adults. A soft-stuffed robot system with a breathing feedback mechanism was designed, modeled, manufactured, and tested. The primary objective was to develop and construct a prototype robot for sleep improvement, which would be tested on real individuals. The proposed soft-stuffed robot incorporated a respiratory feedback system utilizing a contact-less capacitive-based sensor to monitor the user's breathing rate. The bio signal obtained from the sensor was then used to adjust the robot's breathing mechanism, creating appropriate stimulus motions on the user through an artificial respiration imitator. The system overview is depicted in Figure 1.

*Corresponding author.
Email address: fengkpsc@ku.ac.th
doi: 10.14456/easr.2024.31

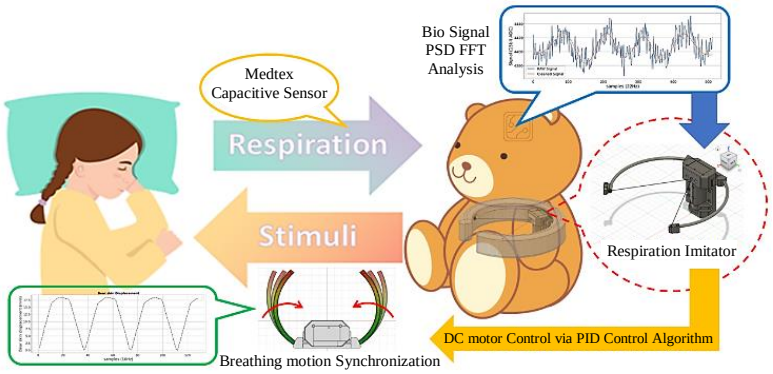


**Figure 1** Overview of the process

## 2. Comprehensive review of therapeutic robots

In this research, the main focus was on designing a stress-induced insomnia robot, considering that humans spend a significant portion of their lives sleeping. Various robots have been developed to mimic the human breathing system, with some researchers proposing therapeutic robots. For instance, a study from Japan introduced Sense-Roid [8], an emotional haptic communication system that provided a simulated hugging experience to the user. Another example is ZZZoo Pillows, a huggable breathing robot designed to simulate sleeping alongside a real human and reduce stress through external breathing stimulation. However, the design of ZZZoo Pillows makes them impractical for use in real human dwellings. Somnox, a bean-shaped robot, can mimic physical breathing cycles and induce a sense of calm, affecting the user's physiological responses. However, it lacks an animal appearance that would make it more appealing to children. Qoobo, an award-winning robot cushion, replicates the purring of a genuine cat through a wagging tail mechanism. While successful in its purpose, Qoobo does not create breathing motion like a real animal when hugged. Additionally, there are several other soft-stuffed robots available in the commercial market, as shown in Table 1.

**Table 1** Summary of commercial therapeutic stuffed robots

| Product | Friendly look | Easy to user | Sensor | Price (USD) |
|---|---|---|---|---|
| Somnox [9] | poor | fair | poor | 590 |
| Qoobo [10] | fair | fair | poor | 400 |
| Flatcat [11] | poor | poor | poor | 500 |
| Furby [12] | fair | fair | poor | 180 |
| Moflin [13] | poor | good | poor | 400 |
| Nicobo [14] | fair | good | poor | 300 |
| Paro [15] | good | good | poor | 5,000 |

In existing robotics research, the emphasis on biometric sensing systems has been lacking. This study aims to address this gap by focusing on the development of a contactless conductive fabric sensor to enhance sensing performance. The improved sensor holds potential for various medical applications, including diagnostic tools and real-time monitoring systems.

## 3. Robot's respiration imitator

The look and feel of the robot were carefully considering in order to relax humans. The soft body robot has benefits over standard hard body robots especially for the stress reduction propose. A teddy bear doll was transformed into a soft-stuffed robot for the prototype by incorporating a mechanical breathing system, a low noise actuator, and a capacitive-based respiration sensor within the doll's internal area. The teddy bear doll used in this study was obtained from the arcade doll picking machine, as illustrated in Figure 2. Internal stuffed cotton was removed to create empty space for robot mechanism. For the research propose, the robot was not controlled by on-board computer, but it was linked to an off-board computer aim for conveniently gathering and processing bio data as well as calculating the control signal. The robot system diagram is shown in Figure 3.

**Figure 2** Teddy bear stuffed toy

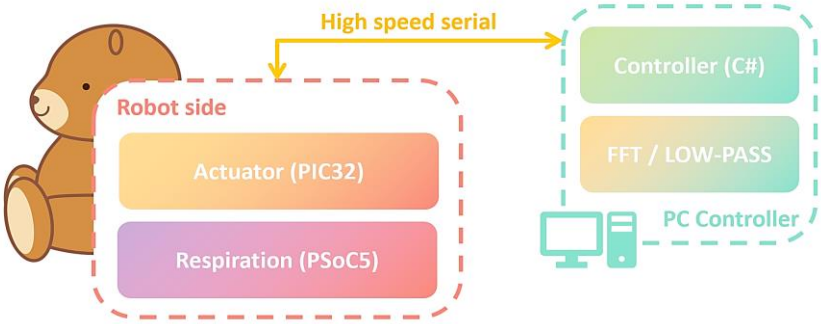


**Figure 3** Stuffed robot system diagram

The development of the breathing mechanism for the soft-stuffed robot posed a challenging task. The main focus was to ensure user-friendliness and comfort. Additionally, the robot system was specifically designed for use during sleep, necessitating a low noise level. To achieve a smooth breathing motion, a flexible robot arm approach was adopted. Flexible 3D materials were utilized to create tubes that acted as robot ribs, while rigid 3D materials were used for the actuator holder component and the robot spine. By manipulating these tubes, the robot could replicate the natural expansion of the lungs and ribs during human breathing. Figure 4 illustrates the respiratory system, which consists of two flexible arms attached to an actuator holding component, functioning similarly to the human spinal system.

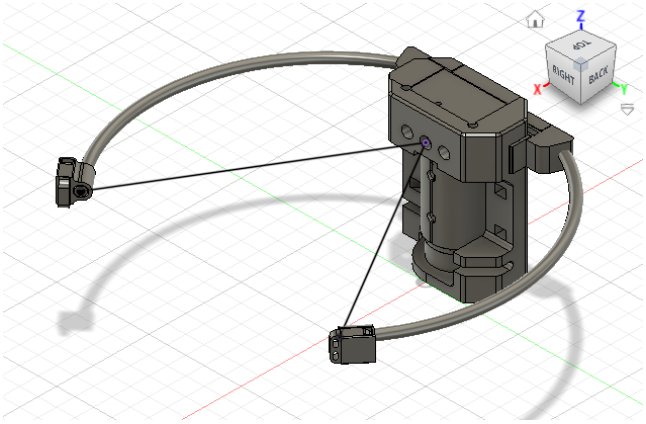

**Figure 4** Designed respiration imitator

The properties and dynamics of the designed imitator mechanism were analyzed using the clamped-mass model of the flexible beam. To simplify the analysis, only one rib arm was initially considered before expanding to the entire system. Figure 5 illustrates the deformation of one imitator rib arm from a top-view perspective. In this imitator structure, a control force was applied at the link tip, generating torque at the hub. The model of this arm was calculated based on the Finite Element Method (FEM). The deformation of the flexible link, $w(x,t)$, generally be much smaller than the link length, $l$, and any extension was neglected, therefore, the flexible arm length can be considered as a constant $l$ for both deformed and undeformed links. The point $x_p$ was considered and can be used to calculate displacement in y-axis as $y_p$ from (1) and the linear velocity of $y_p$ by (2) when the rotated angle $\theta$ and $w(x,t)$ were small or link had a small deflection

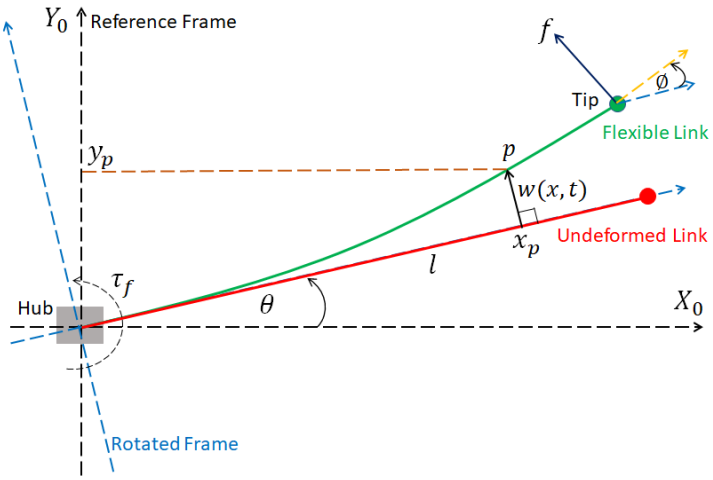


**Figure 5** Free body diagram of the flexible arm

$$y_p = x_p\theta + w(x,t) \tag{1}$$

$$\dot{y}_p = x_p\dot{\theta} + \frac{\partial w(x,t)}{\partial t} \tag{2}$$

The velocity in x-axis of the point $P$ was $w(x,t)\dot{\theta}$. Total kinetic energy of the flexible imitator arm was the combination of the kinetic energy of hub, kinetic energy of link and kinetic energy from tip mass as shown in (3).

$$E_k = \frac{1}{2}I_H\dot{\theta}^2 + \frac{1}{2}\rho\int_0^l\left\{\left(\frac{\partial w(x,t)}{\partial t} + x\dot{\theta}\right)^2 + \left(w(x,t)\dot{\theta}\right)^2\right\} + dx + \frac{1}{2}M_P\left(\frac{\partial w(x,t)}{\partial t} + l\dot{\theta}\right)^2\Big|_{x=l} \tag{3}$$

Where,

$I_H$ is the inertia of the hub.
$\rho$ is the uniform linear mass density in kg/m
$M_P$ is the mass of the tip.

Because the arm was desired to be parallel to the ground, therefore, no potential energy from the gravity. Total potential energy due to elastic deformation of the link is (4). Where, $EI$ is the constant flexural rigidity.

$$E_p = \frac{1}{2}EI\int_0^l\left(\frac{\partial^2 w(x,t)}{\partial x^2}\right)^2 dx \tag{4}$$

Then, the dynamic equation of each arm in the imitator mechanism can be derived from Euler-Lagrange equation of motion as (5).

$$\frac{d}{dt}\left(\frac{\partial L}{\partial \dot{q}_i}\right) - \frac{\partial L}{\partial q_i} + \frac{\partial D}{\partial \dot{q}_i} = \tau_f \tag{5}$$

Where,

$L = E_k - E_p$ is the Lagrangian variable
$D$ is the Rayleigh's dissipation function
$q_i$ is the generalized state variable
$\tau_f$ is the generalized torque

Generally, the generalized force in the robot system according to link variable is torque $\tau_f$ that was applied to the link at the hub. The Rayleigh's dissipation function $D$ allows dissipative effects to be included into the dynamic equation. The dissipative effects accrued when beam absorbs energy from the structure due to its response [16]. The dissipated energy can be written as (6). Where, $C(x)$ is the viscous air damping, $C_s$ is the resistance to strain velocity constant and $C_0$ is the resistance to angular velocity at the tip constant.

$$D = \frac{1}{2}\int_0^l C(x)\left(\frac{\partial w(x,t)}{\partial t}\right)^2 dx + \frac{1}{2}\int_0^l C_s\left(\frac{\partial^3 w(x,t)}{\partial x^2\partial t}\right)^2 dx + \frac{1}{2}\int_0^l C_0\left(\frac{\partial^2 w(x,t)}{\partial x\partial t}\Big|_{x=l}\right)^2 dx \tag{6}$$

The dissipative effects are small and can be neglected, imitator arm had no tip weight and hub did not rotate in order to generate breathing motion, thus, the equation (5) can be derived as (7). The dynamics of the arm requires deformation function $w(x,t)$. The deformation function can be obtained by FEM when assigned proper boundary conditions. The boundary conditions for this flexible arm displayed as (8) to (11). More over the Euler-Bernoulli equation for a beam, for which rotary inertia and shear deformation effects are ignored, was required as the deformation equation of the arm and equal to (12). The torque $\tau_f$ that applied to the arm was introduced by external force $f$, thus, the torque can be obtained as (13)

$$\tau_f = \left(\tfrac{1}{3}\rho l^3 + \rho\int_0^l (w(x,t))^2 dx\right)\ddot{\theta} + \left(2\rho\int_0^l w(x,t)\frac{\partial w(x,t)}{\partial t}dx\right)\dot{\theta} + \rho\int_0^l x\frac{\partial^2 w(x,t)}{\partial t^2}dx \tag{7}$$

$$w(0,t) = 0 \tag{8}$$

$$\frac{\partial w(x,t)}{\partial t}\Big|_{x=0} = 0 \tag{9}$$

$$w(x,0) = w_0 \tag{10}$$

$$\frac{\partial w(x,t)}{\partial t}\Big|_{t=0} = \dot{w}_0 \tag{11}$$

$$EI\frac{\partial^4 w(x,t)}{\partial x^4} + \rho\frac{\partial^2 w(x,t)}{\partial t^2} = 0 \tag{12}$$

$$\tau_f = \vec{f} \times \vec{l} \tag{13}$$

Once the dynamic model of the imitator arm system was derived, the next step involved manufacturing the actual mechanism. Materials of the artificial respiration mechanism must be sturdy but flexible enough to create breathing motion especially for the flexible arm. Given the complexity of the designed imitator system, 3D printable materials were chosen for this research due to their availability and ability to form complex parts. Careful selection of various thermoplastic materials was carried out for the flexible arms structure. To simulate the mechanical behavior of different materials under various usage conditions, a numerical analysis process was employed. The simulations were conducted using Calculix [17], a finite element module within the FreeCAD software [18]. The simulated environment accurately depicted the respirator structure, including the force direction and all relevant characteristics, as illustrated in Figure 6.

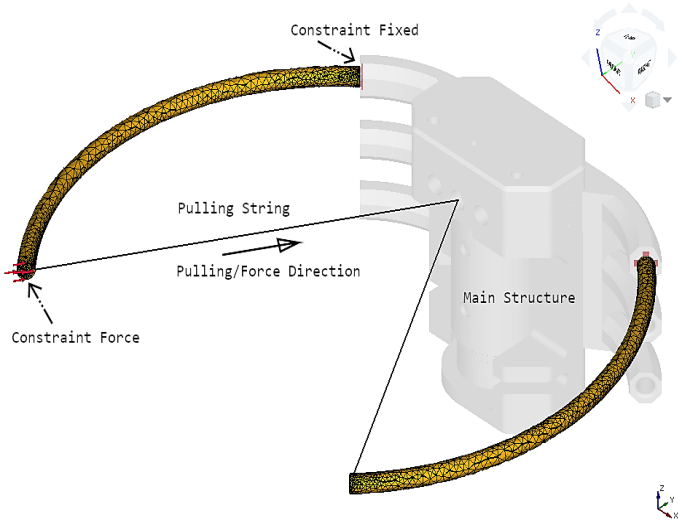


**Figure 6** Criteria of arm simulations

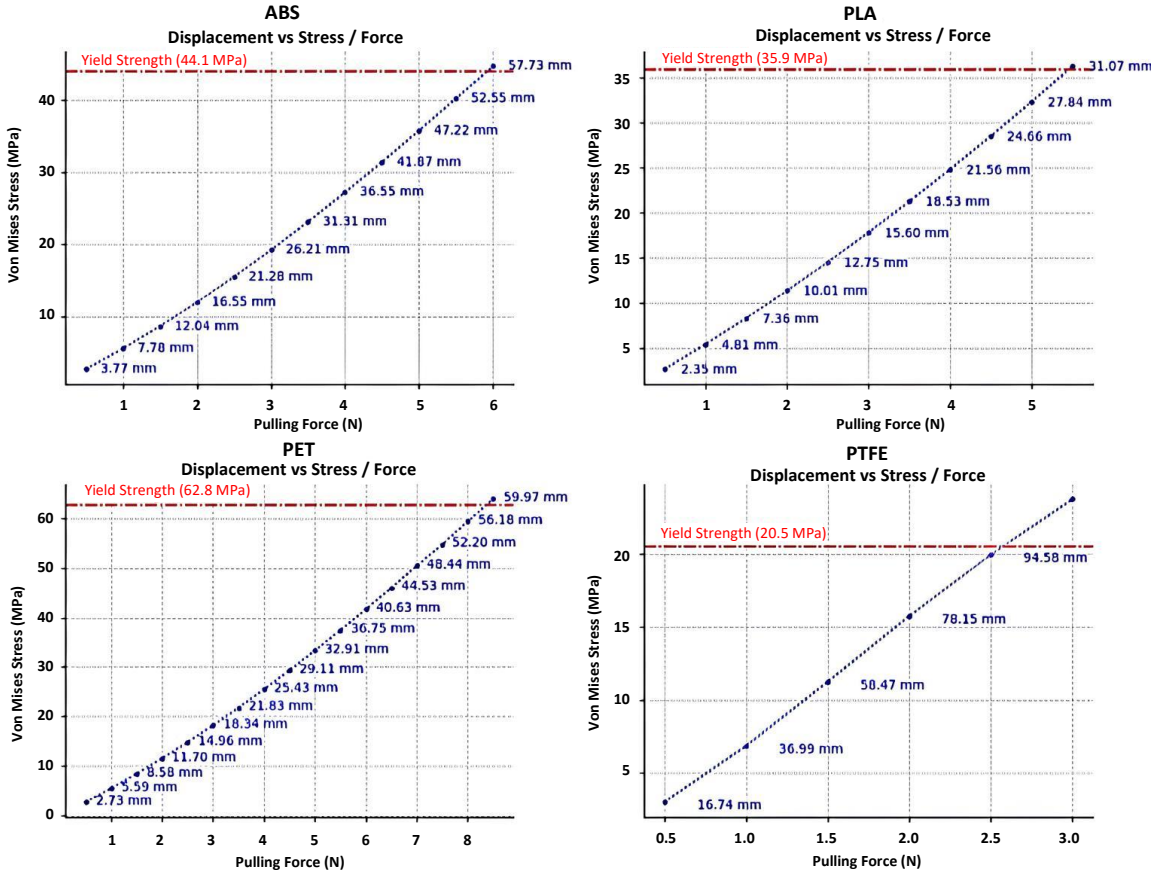


**Figure 7** Simulated result of 3D materials

The selection of appropriate materials for different parts of the respiration imitator was based on their respective workload and responsibilities. To determine the properties of typical 3D printing materials, simulations were conducted on popular thermoplastic materials, as depicted in Figure 7 under the influence of external forces. The simulation results guided the selection of suitable materials for each component of the imitator. The core body structure served as the support for all system components, including electronics and sensors. It needed to be strong enough to withstand the force and heat generated by other parts while securely holding them in place. Therefore, ABS was chosen to construct the basic body structure. Auxiliary pieces, such as joint locks, snap locks, and arm tip connectors, were required to connect various portions to the core body structure. These pieces needed to be flexible yet sturdy, without requiring high heat resistance. Based on the simulation findings, PLA was selected as the material for these auxiliary parts. Its strength, flexibility, and ease of forming, as demonstrated by its adhesion properties, made it ideal for this purpose. The robot ribs and arm were vital components that facilitated a gentle breathing motion and provided a delicate touch for the user. These components demanded materials with high flexibility and the ability to restore their shape during the breathing motion. Considering its excellent flexibility and good recovery after compression, PTFE was chosen for the ribs section. An overview of the materials used for the respiration mechanism is presented in Figure 8. Based on simulated result, a robust actuator for an imitator core was required. Among high performance actuators, a customized RE-max series from Maxon Motor was selected due to its properties as shown in Table 2. This motor can create 15.6 mNm of continuous torque thanks to the powerful neodymium magnet core.

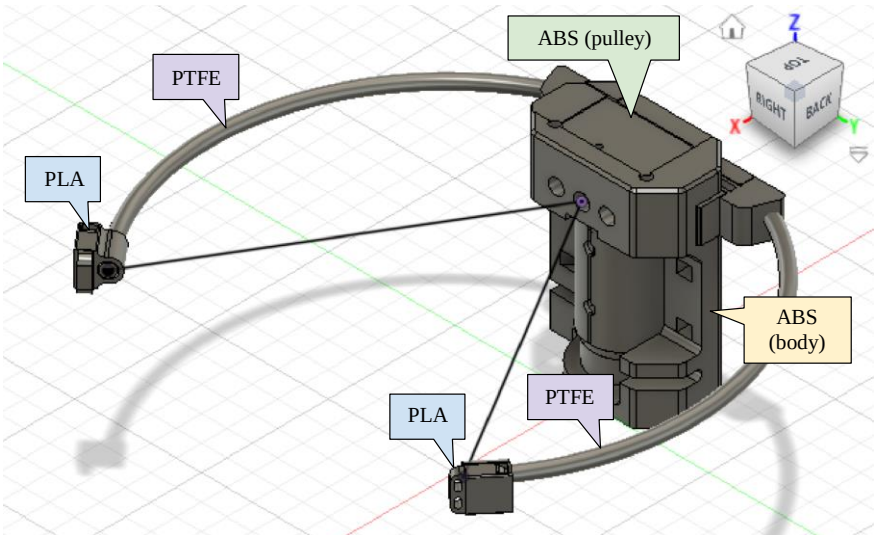


**Figure 8** Detail of the respiration imitator materials

**Table 2** RE-Max Maxon motor parameters

| Parameter | Unit | Value |
|---|---|---|
| Nominal voltage | V | 12 |
| No load speed | rpm | 6010 |
| No load current | mA | 23.6 |
| Nominal speed | rpm | 5430 |
| Nominal torque (max. continuous torque) | mNm | 15.6 |
| Nominal current (max. continuous current) | A | 0.84 |
| Stall torque | mNm | 156 |
| Stall current | A | 8.22 |
| Max. efficiency | % | 90 |
| Terminal resistance | Ω | 1.46 |
| Terminal inductance | mH | 0.108 |
| Torque constant | mNm/A | 19 |
| Speed constant | rpm/V | 502 |
| Mechanical time constant | ms | 4.42 |
| Rotor inertia | $gcm^2$ | 10.9 |

The motor is the brushed type motor that comes with a build-in encoder that attached to its back for precision control and the motor shaft position can be controlled by PWM signal. However, to accurately simulate real human breathing, a more sophisticated respiratory mechanism was required, demanding extreme precision. Therefore, an advanced method for measuring the motor angle with high accuracy was necessary. A sheet-shaped rubber magnet was mounted to the tip of the motor shaft just above an additional hall effect sensor. Thus, the magnetic flux density of the two axes perpendicular to the rotating axis could be measured using a magnetic sensor, which was counted by A/D converter of the microcontroller to obtain the motor angle as shown in Figure 9.

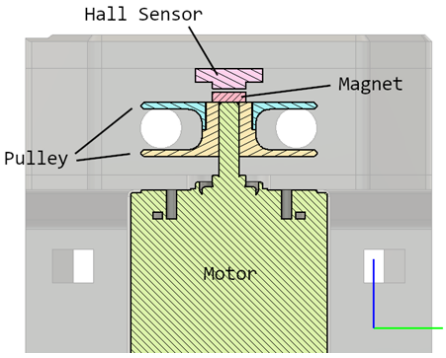


**Figure 9** A cross section of magnetic sensors structure

The Giant Magneto Resistance (GMR) sensor, TLE5009 from Infineon Technologies [19] had been chosen in this research to measure the magnetic flux. The sensor and magnet were contactless in order to reduce the damage from frictions that can occur when motor was operated. A robot controller board, NUIBOT [20], was selected for string driven soft mechanism. This controller board was designed specifically for stuffed-toy robots. The main microcontroller is the PIC32 MM0064 GPL036. To control the motor, the controller board receives an instruction from the host computer using Universal Asynchronous Serial Communication, or UART protocol. Host computers send breathing motion trajectory to the controller board and the controller generate the PWM control signal to the motor with feedback from the magnetic sensor. The control algorithm was designed based on a digital Proportional Integrator and Deferential or PID controller with position feedback from magnetic data. The magnetic flux from the pulley is measured as shown in Figure 10. By controlling the rotational speed and angle of the pulley, respiratory motion can be achieved. In addition, the motor driver consists of two DRV8833 motor driver chips from Texas Instruments with current measuring feature [21]. This driver can drive current up 1.5A at 10.8V. Because the highest weight that human fingers can hold is around 5 kg, the 0.8 thickness thread is used for pulling the imitator core for the safety. This thread can withstand a maximum weight of 4.8 kg. The controller board was installed into the robot imitator backbone for compact and shown in Figure 11.

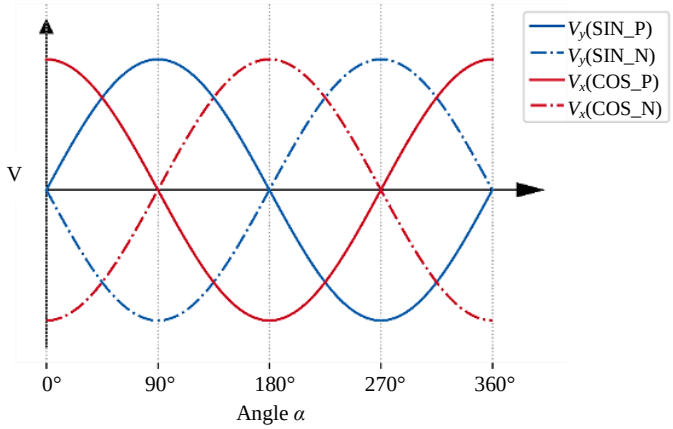


**Figure 10** TLE5009 measurement of the magnetic field direction

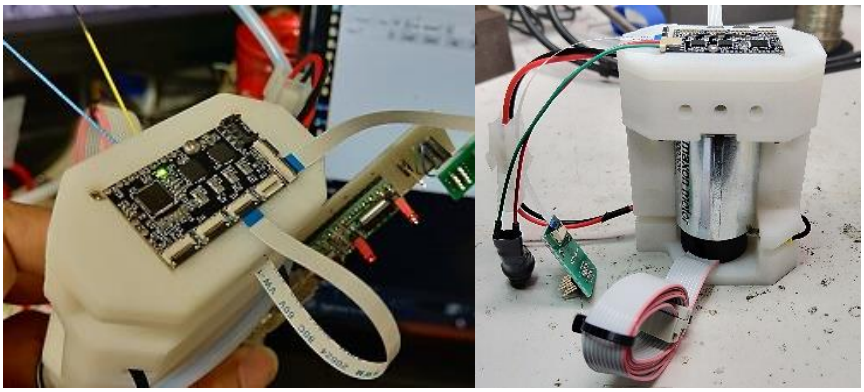

**Figure 11** Controller board and the complete robot backbone

In order to confirm the properties of the selected material, the experiment was setup. The complete imitator system was driven by the actuator and the driven force was corrected via driving current that flew into the motor. Then, the captured driven force was applied to the simulation environment and the result was recorded. The displacement and blend of the imitator arm between the real system and the simulation were compared as shown in Figure 12. There was a small different between the real imitator and the simulation because of the arm tip parts that were attached to the arm create the extra masses.

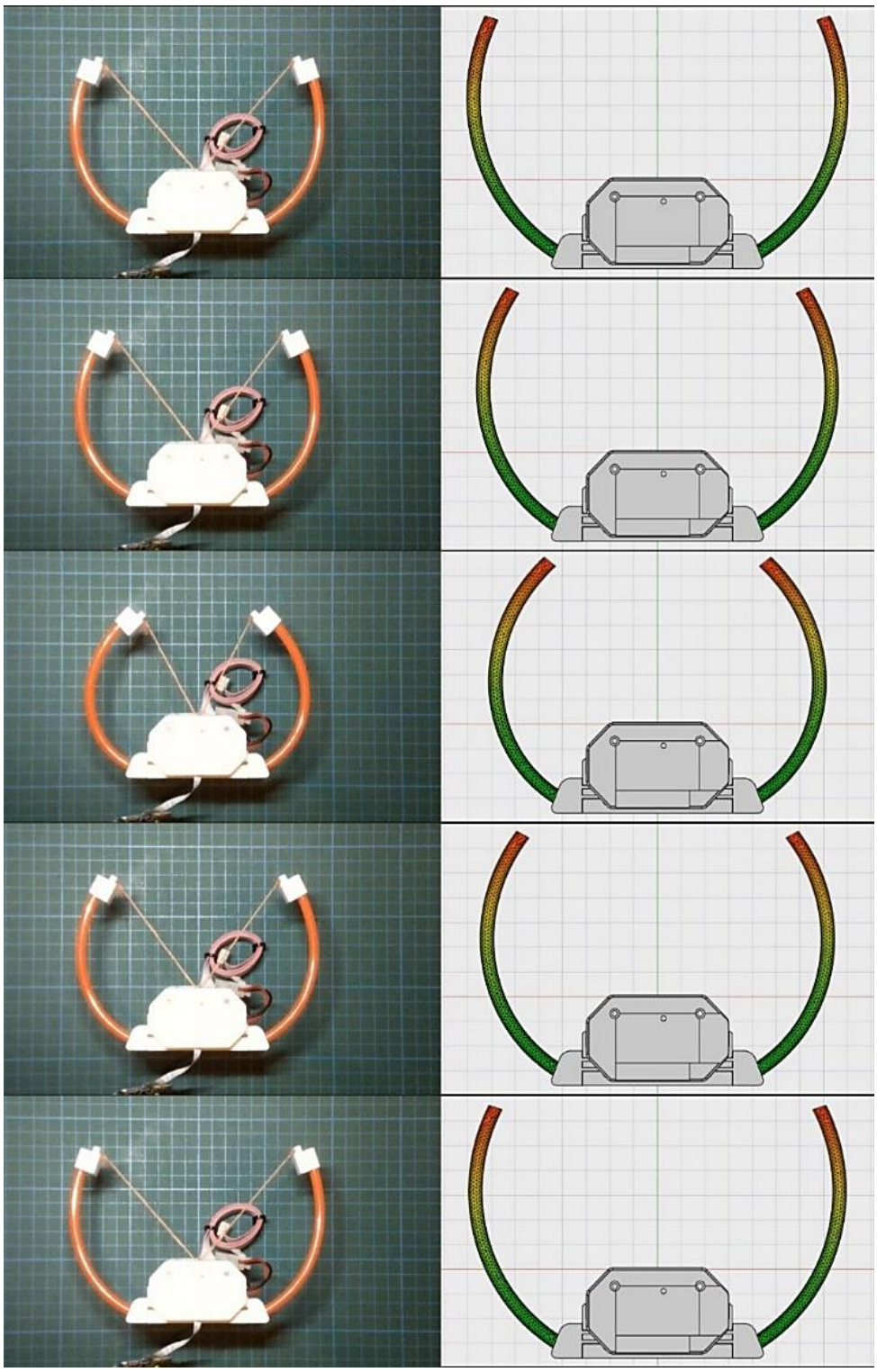

**Figure 12** Comparison between the real imitator and the simulation with the same driven force (Top view)

The softness of the robot's exterior was an important consideration in the design process. The imitator's structure was carefully designed to mimic the human thorax, with the ribs playing a crucial role. These rib-like structures supported the expansion mechanism and prevented the collapse of the outer exterior during breathing movements. At the center of the backbone, an actuator system was installed. This system began with the actuator located at the body core, which could generate maximum torque. The torque was then transmitted to the pulley positioned at the center of the core. Dual V-shaped strings were attached to the pulley and extended to the tip of the arms. The timing and trajectory of the actuator could be controlled by the controller circuit at the top of the actuator system. To imitate the human ribs, the designed imitator arms were enclosed by a cushion pillow. This pillow not only provided a soft touch but also concealed the underlying robot structure, creating the illusion of soft tissues. Additionally, the cushion pillow ensured that the robot maintained its shape and prevented deformation when the user interacted with it, such as through hugging. This combination allowed for a realistic and tactile experience for the user. Finally, all the robot parts were installed within the teddy bear doll skin, as depicted in Figure 13.

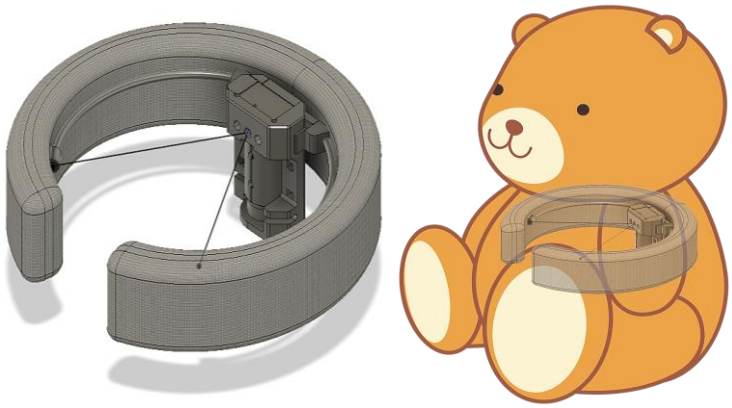

**Figure 13** Soft pillow attached to the imitator mechanism and installation

After the robot has been completely assembled, its safety in use was tested especially for volatile chemicals. The glass transition temperature was considered because at this temperature, the material begins to transform from a solid to a glass state. At this condition, the material becomes brittle like glass, and volatile chemicals may be created. Table 3 shows the material properties of the robot imitator system. PLA has the lowest glass transition temperature at 60 °C. The operational temperature of the robot when the dc motor is turned on was measured. The robot was tested in an air-conditioned area to simulate the actual bedroom atmosphere. The highest temperature within the robot is around 39°C surrounding the motor; thus, the temperature of the auxiliary parts at the end of the rib is lower than that of the motor. This auxiliary part was made from PLA, and its operating temperature is lower than its glass transition temperature. By considering this information, the robot is safe to use.

**Table 3** 3D materials properties

| Parameter | ABS | PLA | PETG | PTFE |
|---|---|---|---|---|
| Odor | Mild plastic | Slightly sweet | Mild | Odorless |
| Glass transition temperature | 105 °C | 60 °C | 85 °C | 126 °C |
| Unsafe temperature range | > 250 °C | > 230 °C | > 260 °C | > 350 °C |

**4. Breathing sensor**

Another difficulty in this research is how to detect the respiration signal. Several affordable biometric studies were conducted in order to determine the optimum com-promise for producing the commodity sensor. According to our studies, in order to detect human respiration in the soft-stuffed robot application was not a simple task be-cause of the materials and noise from users. Not only the softness of the material was matter, but also the user's comfortable was important. In this topic, the selecting of the respiration detection system was explained.

In order to achieve a non-invasive sensor design for monitoring the respiratory system, various sensor options were explored. A proximity detector was initially tested to capture respiratory movements. Previous research [6] proposed an expandable sensor method for monitoring breath expansions, but it was not suitable for use in soft stuffed robots due to its strap-like design, which may not be user-friendly. Another method called Capaciflector [22] involved creating an inductance beam to detect biometrics from human reflexes. However, our studies indicated that a delicate analog circuit would be required to generate a precise detecting signal, which may not be practical for use during sleep or in real-world applications. Next, CapSense technology from Cypress Semiconductor [23] was explored. This sensor allowed for the detection of tiny changes in capacitance, such as those associated with human respiration. With its built-in Delta-Sigma Modulator, the sensor provided versatile and efficient signal compensation, capable of monitoring differentiation of inductance changes. A single plate of insulated copper was used as a shield electrode, which was connected to the microcontroller using shielded wire. By receiving the periodic signal propagated from the CapSense circuit, the microcontroller could capture changes in inductance. When a large inductance object, such as the human body, was present, the inductance in the shield electrode would change and could be sensed by the circuit. The system's automatic tuning procedure allowed for adaptation of parameters to different shapes, sizes, and types of conductive materials used in the shielded electrodes. However, it was found that although the sensor had a good response, it could not be used in a soft-stuffed robot due to its rigid nature and difficulties in installation, which could create discomfort for the user.

To ensure the creation of a comfortable and well-functioning soft stuffed robot, careful selection of soft materials and sensors is essential. However, installing a large shield electrode into a soft-stuffed robot may not be suitable, which led to the consideration of conductive textiles for this purpose. Among the available options, Shibata conductive cotton was initially chosen for experimentation. This textile is made from copper threads combined with cotton thread, woven using an alternating weaving system. It is commonly used for power distribution in e-textile applications. Unfortunately, the results showed that the conductivity of the copper thread structure was not sufficient for the intended purpose. Finally, Medtex 180 Ag Nylon single directional stretch fabric [24], as shown in Figure 14, was selected. This conductive knit fabric is also used in e-textile applications. It is composed of silver-plated nylon and has a stretchy property in one direction. With a surface resistivity of less than 1 $\Omega$/sq, it exhibits high conductivity. This textile proved to be an excellent candidate for capacitive and flexible applications. An experiment was conducted to test the conductivity and sensitivity of the Medtex textile, as depicted in Figure 14.

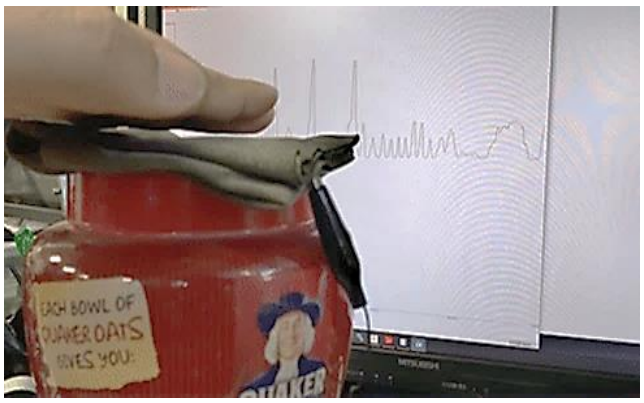


**Figure 14** Conductivity and sensitivity experiment on Medtex 180 Ag Nylon

## 5. Robot software

A precise software system was necessary to control the sophisticated hardware of the soft-stuffed robot. For simplicity and flexibility, the software was implemented on the host computer rather than in the embedded system of the robot. This allowed for easy code changes and facilitated experimentation. The software was divided into sub-modules, including the control unit, motor control unit, and sensor signal processing unit. All units' codes were developed using the C# language and the .Net framework software development kit. The motor control unit was assigned to communicate and control the motor driver board. Based on the original NUIBOT control software, the communication to the driver was made by sending and receiving the custom binary-encoded message package via the high-frequency continuous synchronous serial communication (UART). The binary-encoded message had the advantage of compact data compression and high-speed data interchange.

At the initiation process phase, the software would send a checking message for obtaining the present status of the driver board and waiting for the feedback message from the driver board before furthering the configuration. When the driver was ready, the configuration would be sent to driver board for configuring an actuator and magnetic sensors. The software reconfigured all the parameters and update the user interface at this stage. Then, the software entered the operation phase. At the operation phase, software communicated with a motor driver by using control message based on PID controller which contains the motor status and the control command message. This allows a closed-loop control algorithm possible. In the same time, bio signal from the capacitive fabric sensor captured human chest motion and this signal was used as the feedback signal to synchronize the robot and human breathing frequency and phase. The respiratory activity signal was cleaned by the low-pass filter before passed it through the Fast-Fourier Transform algorithm to predict a respiration frequency. Then the result was used in the feedback algorithm for calculating the response motion for the actuator. However, this approach was rich in calculation since it required both low-pass filter and FFT transformation. The experiment was conducted to testing the performance of the designed robot system. The user interface (UI) dashboard, as depicted in Figure 15, displayed raw data and its spectrum.

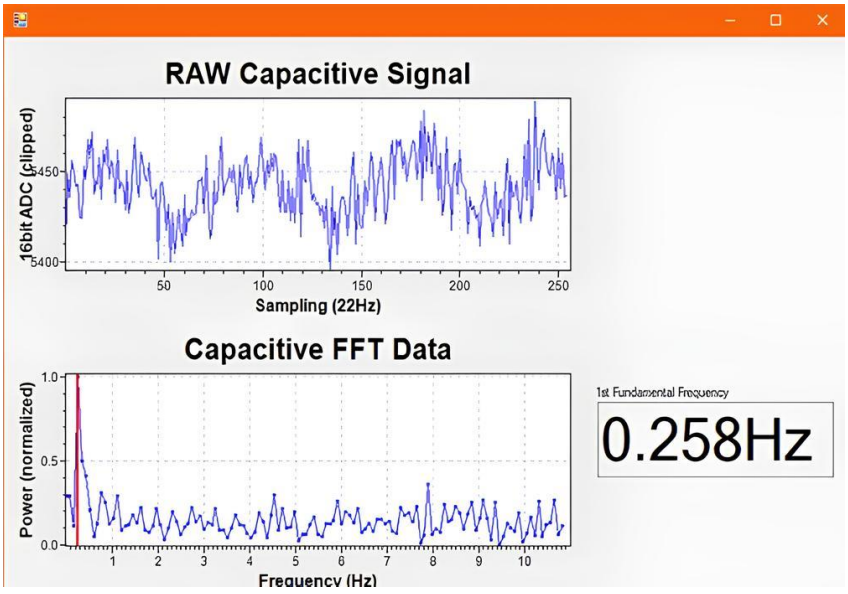


**Figure 15** Raw signal (top) and FFT spectrum (bottom) captured from human body

## 6. Experiments

The soft-stuffed robot was manufactured using the designated mechanism materials and a bear doll skin. All the components were installed in the robot body and tested for breathing motion. Prior to the human experiment, a comprehensive performance test was conducted on the completed soft-stuffed robot system. In this experiment, the actuator drove the repository imitator with a cyclic angular trajectory to simulate human breathing motion, as illustrated in Figure 16. The displacement of the bear doll skin was recorded

and depicted in Figure 17. The results of this experiment demonstrated that the designed robot successfully achieved the desired breathing motion, with the doll skin moving up to a difference of 17.8 mm between inhale and exhale motions. Furthermore, the impact of the doll skin on the imitator was assessed by comparing the achievable angle of the motor with and without the imitator installed inside the doll shell. The experimental results, shown in Figure 18, indicated that the angle of the motor differed by approximately 6.81% when the imitator was installed in the doll compared to when it was operated outside the doll. This experiment confirmed that the selected actuator generated sufficient force for the imitator to generate the breathing motion.

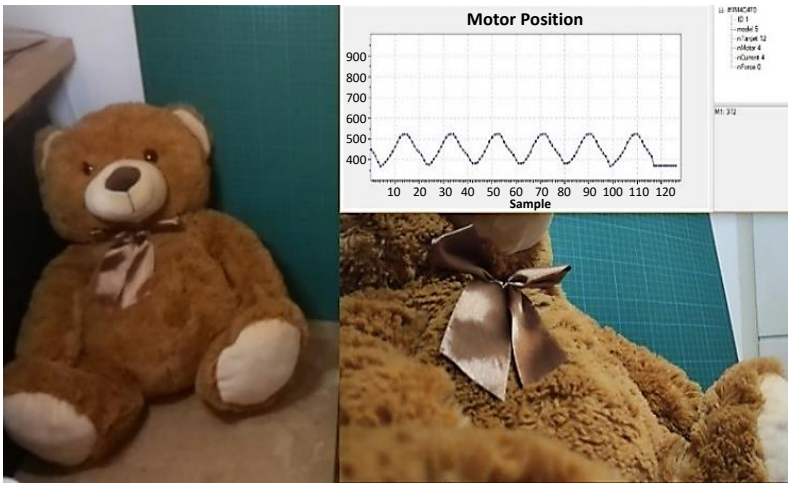


**Figure 16** Robot's breathing motion

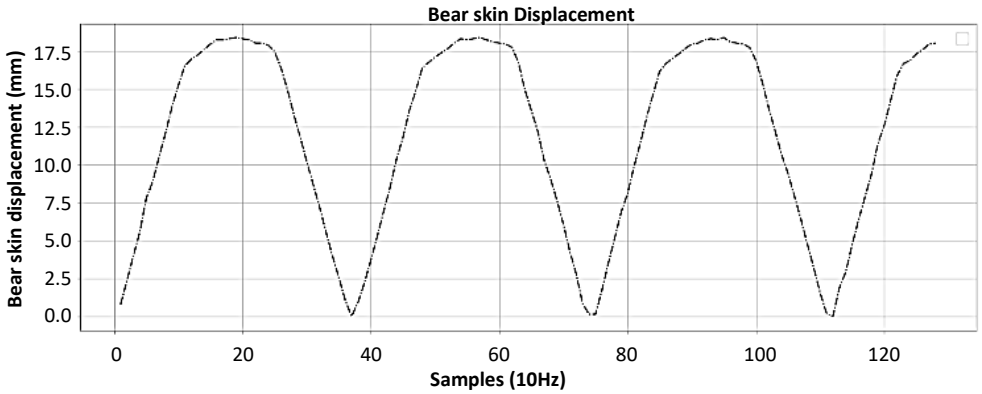


**Figure 17** Robot skin displacement

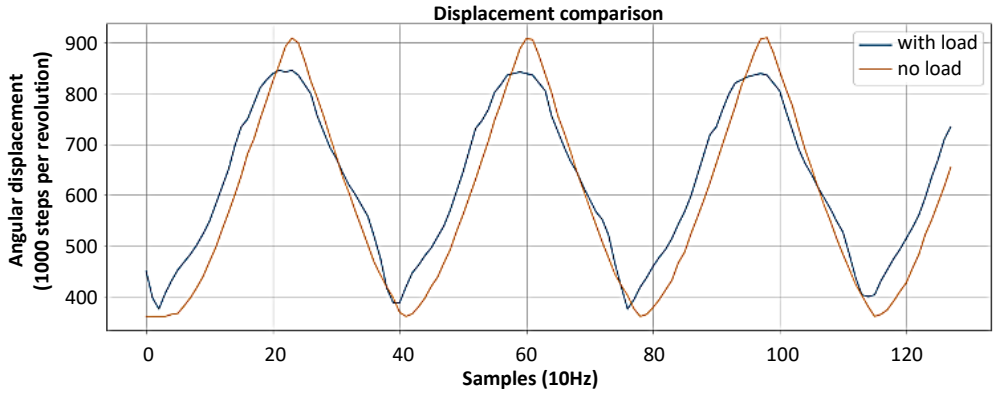


**Figure 18** Comparison of motor angle achieved with and without load

Subsequently, human experiments were conducted during nighttime to simulate a real-life scenario. The aim was to capture the human bio signal and obtain the breathing signals, in order to analyze the human respiration period and predict their sleeping pattern. The experiment was set up in a bedroom, with the robot connected directly to a desktop computer. The volunteer was kindly asked to hold the robot while sleeping, as depicted in Figure 19. The breathing motion of the volunteer was monitored using a capacitive proximity sensor embedded in the robot's chest. Throughout the night, the experiments continuously collected raw sleeping data signals. The volunteer was instructed to embrace the robot near their respiratory system. For this research, the observation period selected was 30 minutes between 4:00 am and 4:30 am. The collected signals were later analyzed offline. Periodic signals were translated into respiration measurements using frequency analysis. By setting appropriate frequency windows and sampling rates, a fundamental frequency component was identified from the signal, approximating the respiration rate.

**Figure 19** Experiment on the volunteer during the night time

Bio-signals always contained noise and the strength of the signal was depended on the location of the sensor to the human body. The distance obtained by measuring the distance changes with the time of the distance between the robot and the user's chest may cause the noise and dc bias shifted. In order to avoid this problem, the frequency domain analysis was used to analyze the bio-signals from the human in this experiment. Thanks to the Fourier Transformation, the time domain signal could be transformed to frequency domain information and it could withstand the different hugging postures and distance caused by moving during sleep deformation or noise from the environment. The sliding mode Discrete Fourier Transform (DFT) was performed throughout the session to extract insights pieces of information before being handed to the observer. Supplement the measurements, the Power Spectral Density (PSD) was calculated over the signal window to obtain a more informative metric for offline observation. PSD was the power of each harmonic in signal frequencies by calculating the square of the magnitude from Fourier coefficients. PSD from the DFT of the signals, in general, showed the amount of each frequency across all bandwidth in the frequency domain. The normal human respiration rate in this case was around 0.2 to 0.3 Hz. By performing a numerical cut-off at only the desired frequency, the higher frequency component caused by soft sensor deformation and environmental noise could be re-moved. The performance of the PSD to noise and dc offset was shown in Figure 20.

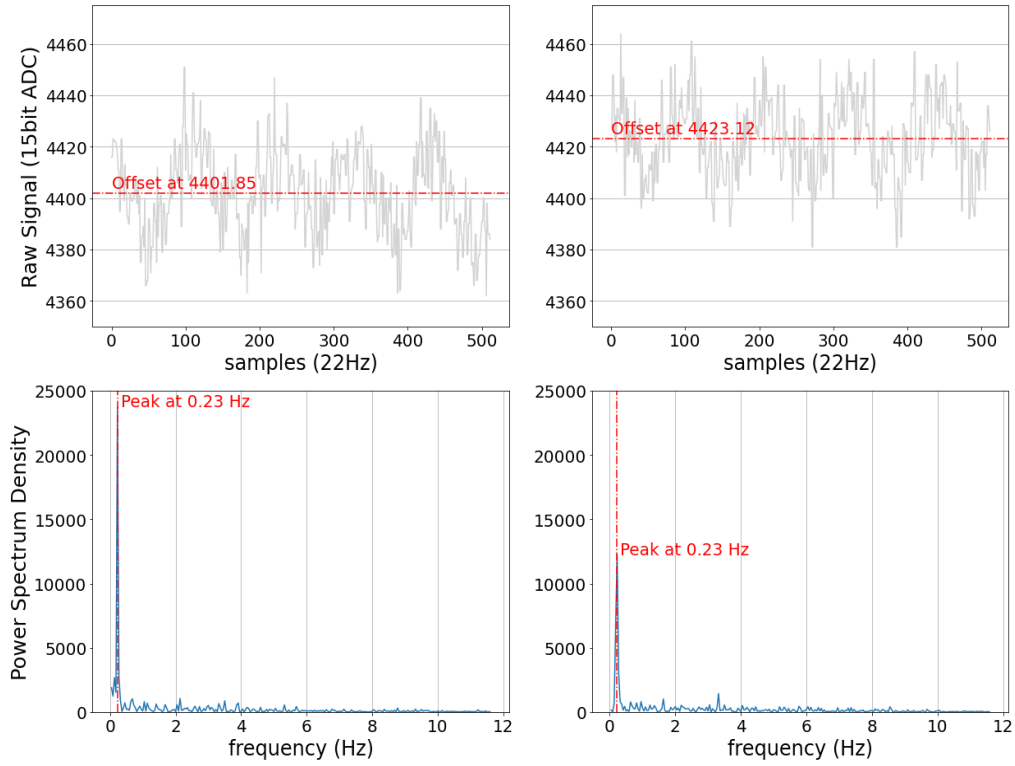


**Figure 20** PSD signal from the experiment

A captured raw data presented an interesting signal pattern that reflected the volunteer's sleep activities. Referred to Figure 21, the captured signal can divide into several sections where the periodic data share the same behavior. The signal can be divided into seven sub-sections as 1, 2, 3, 4, 5, 6 and 7 as shown in Figure 21. Each section was analyzed with a combination of the raw signal, DFT, and PSD information in combination with clinical reports. For an informative description, we described the following results in form of chronological events.

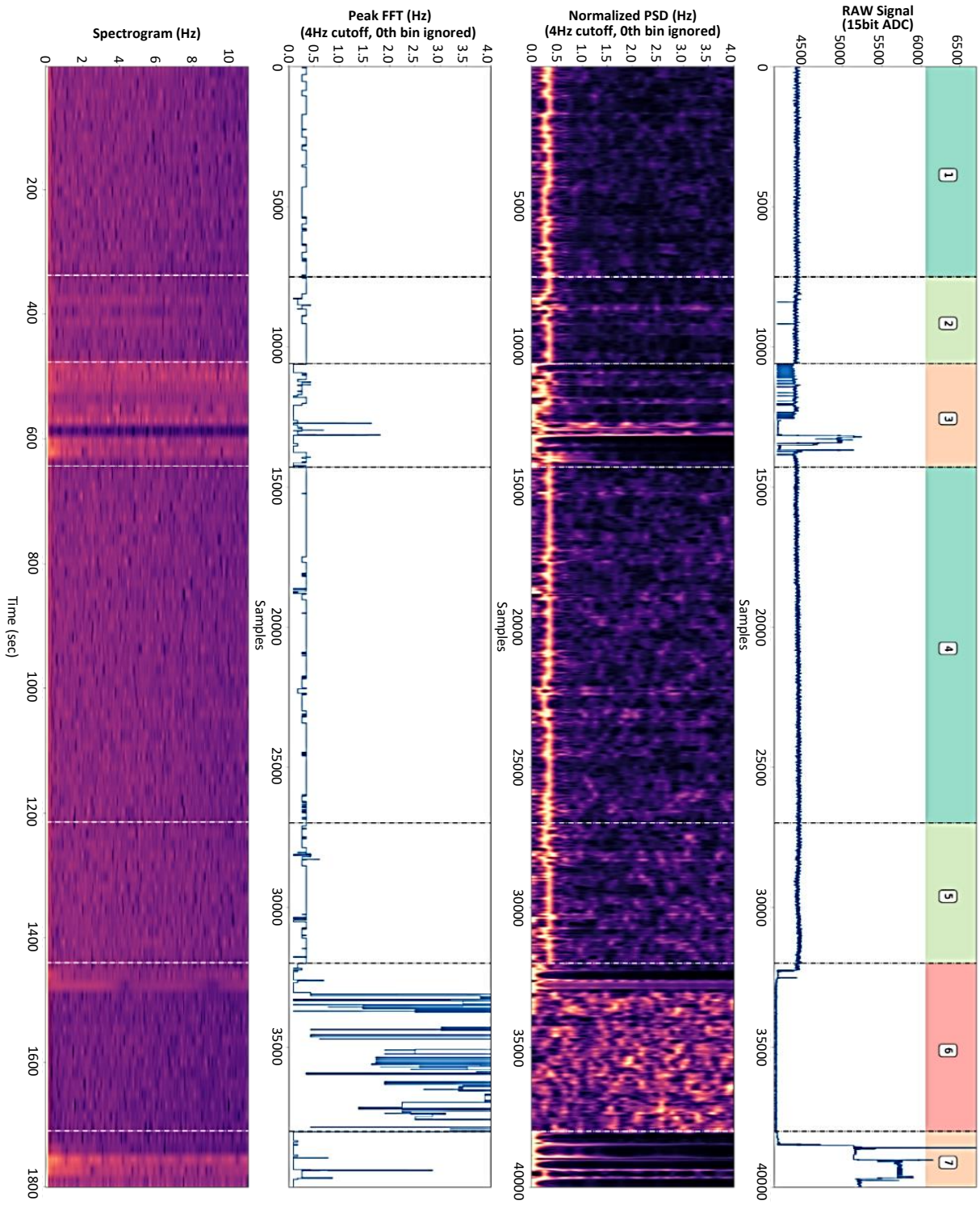


**Figure 21** Sleeping signal segment of 30 minutes. (Time: 4:00 am to 4:30 am)

Section 1, as highlighted by the green color, represents the most common stable sleep behaviors observed. This section occurs when the volunteer maintains a steady-state sleep for an extended period, with a respiration rate ranging from 0.2Hz to 0.3Hz, approximately 12 to 18 breaths per minute. These findings align with previous clinical studies, which indicate that the average respiration rate during sleep for a healthy adult fall within the range of 12 to 20 breaths per minute. Furthermore, the frequency spectrum analysis reveals low turbulence in the power components, as evident in both the FFT and PSD plots as shown in section 2. It exhibits peak frequency along with signal disturbances in the time domain. This period is classified as a preconscious sleep phase, denoted by the light-green color. It frequently occurs before abnormal sleep activities manifest. Initially, the respiration rate slightly decreases from the average, or additional oscillations are observed in the very low-frequency spectrum. While there may be no significant difference in the power spectral density (PSD) compared to the previous section, the FFT analysis demonstrates notable changes.

Then, in Section 3, a significant change is observed, indicated by the orange color. During this period, the volunteer becomes conscious and attempts to adjust themselves to a more comfortable sleep position, often following uncomfortable sleep postures. Interestingly, this section reveals a distinct pattern in the signal structure. The turbulence observed in the FFT analysis is a result of fluctuations in the volunteer's movements. Additionally, the power in the PSD spreads to adjacent frequency bands, indicating an

overall change in peak frequency. This finding is crucial as it demonstrates the proper functioning of the capacitive sensor in accurately capturing a range of values. Furthermore, this occurrence can be indicative of an abnormal sleep state. Such information can be utilized to assess overall sleep quality, duration, or even predict potential conditions such as Restless Leg Syndrome [25]. After the body adjustments, the volunteer returns to a stable sleep position, initiating a new sleep cycle, as depicted in section 4. It is worth noting that the peak FFT displays slightly higher respiration rates, accompanied by an increase in higher frequency noise across the range of this section. This indicates that the volunteer may not have fully reached a steady state of sleep, as an unstable breathing pattern is observed. The observation continues until section 5, where significant fluctuations are observed in both the time domain and the FFT due to a large breathing movement by the volunteer. This type of transition provides valuable insights for health monitoring, as notable changes in respiratory rate can be indicative of other abnormal activities or diseases such as ineffective gas exchange or cardiac arrest caused by cerebral hypoxia [26]. Interestingly, the system can monitor such transitions without difficulty.

Section 6, represented by the red color, exhibits a sudden drop in the signal and the introduction of high-frequency noise in the FFT analysis. In this period, it is challenging to determine the specific activity without additional data from the power spectral density (PSD). Notably, we observe the lowest power across all spectrum bands compared to other periods in the session. This suggests that the fabric sensor was positioned too far from the detection surface (in this case, the human breast), resulting in the collection of environmental noises from the surrounding open space. The observer noticed that during section 5 and the beginning of section 6, the volunteer experienced discomfort due to Nocturia, which is one of the sleep disorders. Subsequently, the volunteer abruptly regained consciousness and woke up from the bed. Once the volunteer returns to the experimental bed, the signal enters section 7. The volunteer returns to the bed and attempts to restore the experimental setup. The sensor is now able to detect the inductance of the volunteer's body. However, the system encounters difficulty in retrieving raw periodic signals within the range of human respiration. This is a consequence of the high inductance of the surface, which occurs when the sensor is placed too close to the volunteer's body. This issue can be attributed to the deformation of the robot's body or excessive constriction. It is worth noting that such limitations are commonly observed in various soft sensors and necessitate improvement in future versions. However, the observation of the signals in the experiment yields several significant pieces of information.

To evaluate the performance of the designed soft robot, a final experiment was conducted. The experiment involved asking the volunteer to sleep under three conditions: without a robot doll, with a robot doll that was not powered, and with a robot doll running in operation mode. The sleep duration was recorded using a commercial wearable device called Amazfit Bip. This device utilizes the STM32L476JEY6 ARM Cortex-M4 microcontroller running at 80 MHz. Bio-signals were measured using an accelerometer model LIS2DH12 and a vital sign module AS7024. These measured signals were combined to approximate the sleep states. The results of the sleep experiment are presented in Figure 22. The experiment revealed that, on average, the volunteer slept for approximately 8 hours and 16.5 minutes when not hugging a robot doll. When the volunteer hugged a robot doll without power while sleeping, the sleeping time increased to an average of 8 hours and 58 minutes. The sleeping time further increased to an average of 10 hours and 3.5 minutes when the robot doll was programmed to simulate breathing. Based on these experimental results, it can be concluded that the robot doll can enhance the volunteer's sleep quality with or without power, but the improvement in sleeping time was significantly greater when the robot doll simulated breathing. During the experiments where the volunteer held a robot doll while sleeping, the breathing cycles were recorded by both our doll and the commercial wearable device. The breathing frequency measured from our doll ranged between 0.2Hz to 0.3Hz, with an average breathing frequency of 0.23Hz. The commercial wearable device recorded an average breathing frequency of 0.26Hz. Therefore, the doll demonstrated an accuracy of approximately 88.47% in measuring the breathing rate compared to the commercial wearable device. Although the results indicated an improvement in sleep duration with the robot doll, the increased sleeping time alone is not conclusive evidence of stress relief caused by the doll. To assess human stress, electroencephalography (EEG) can be used, but it requires measurement by trained physicians in a hospital setting. This would provide a more comprehensive understanding of the real effects of the designed robot doll on humans. Unfortunately, full clinical trials could not be conducted in hospitals, and the sleep laboratory capacity was limited in terms of both manpower and equipment. Based on the research aim of exploring the potential of robots to enhance sleep quality, the experiment demonstrates promising indications of the possibility to improve sleep through the use of a robot.

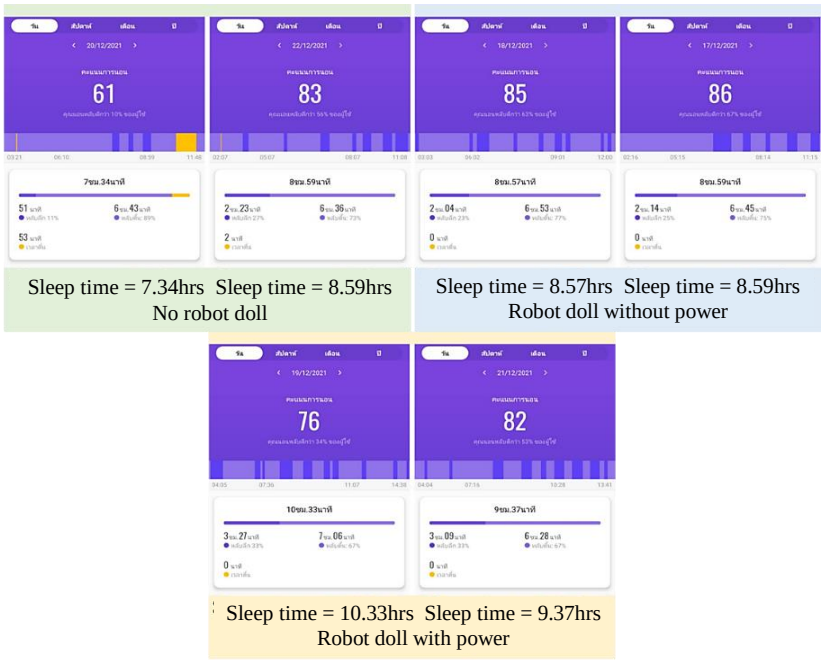


**Figure 22** Experimental result of the sleeping experiment

At this point, the sensor detects the inductance of the volunteer's body. However, the system is unable to retrieve raw periodic signals within the range of human respiration. This is due to the high inductance of the surface, likely caused by the deformation of the robot's body or excessive proximity to the volunteer's body. Such limitations are commonly encountered in various soft sensors and will need to be addressed and improved in future iterations.

## 7. Conclusion and future work

This research aimed to explore the potential of using a soft robot to enhance sleep quality by mimicking the comforting effects of hugging a human or animal. A soft-stuffed breathable doll was introduced as a solution, designed with a feedback bio-signal to determine sleeping states. Multiple prototypes of the robot were developed, including artificial lung functioning and a breathing imitator mechanism. The robot ribs were created using 3D printing techniques and suitable materials, with Medtex 180 AG nylon fabric for conductive sensing. Experiments involved volunteers holding the robot while sleeping, with data processed to separate sleep activity into seven sub-sections. The capacitive sensor system accurately predicted respiration rates, demonstrating the possibility of sleep time improvement. The designed breathing sensor used frequency domain analysis to address signal distortions. The experimental result suggests promising possibilities for improving sleep quality using the designed robot. The experiment showed that holding a powered robot doll increased sleep time by approximately 2 hours for the volunteer. Unfortunately, full clinical trials were postponed due to limitations of resources. The proposed robot system has potential applications beyond sleep improvement in healthcare contexts. This type of robot could assist in personal health care, monitor vitality, and provide relaxation techniques like meditation to reduce stress. Robot system could be improved in the future by adding moisture-enhanced breathing air module in the breathing area for extra medication especially for users who have respiratory issues.

## 8. Acknowledgements

This research is supported under research fund of RobotCitizen laboratory, Faculty of Engineering, Kasetsart University; as well as hardware and technology supported by Hasegawa Shoichi Laboratory, Precision and Intelligence Laboratory, Tokyo Institute of Technology.

## 9. References

[1] Glaser R, Kiecolt-Glaser JK. Stress-induced immune dysfunction: implications for health. Nat Rev Immunol. 2005;5(3):243-51.
[2] Black DS, O'Reilly GA, Olmstead R, Breen EC, Irwin MR. Mindfulness meditation and improvement in sleep quality and daytime impairment among older adults with sleep disturbance: a randomized clinical trial. JAMA Intern Med. 2015;175(4):494-501.
[3] Allen KM, Blascovich J, Tomaka J, Kelsey RM. Presence of human friends and pet dogs as moderators of autonomic responses to stress in women. J Pers Soc Psychol. 1991;61(4):582-9.
[4] Odendaal JS. Animal-assisted therapy - magic or medicine?. J Psychosom Res. 2000;49(4):275-80.
[5] Ballarini G. Pet therapy Animals in human therapy. Acta Biomed. 2003;74(2):97-100.
[6] Shibata T. Therapeutic seal robot as biofeedback medical device: Qualitative and quantitative evaluations of robot therapy in dementia care. Proc IEEE. 2012;100(8):2527-38.
[7] Libin AV, Libin EV. Person-robot interactions from the robopsychologists' point of view: the robotic psychology and robotherapy approach. Proc IEEE. 2004;92(11):1789-803.
[8] Takahashi N, Okazaki R, Okabe H, Yoshikawa H, Aou K, Yamakawa S, et al. Sense-Roid: Emotional haptic communication with yourself. Proceedings of Virtual Reality International Conference (VRIC 2011); 2011 Apr 6-8; Laval, France. New York: ACM; 2011. p. 1-4.
[9] Somnox. Somnox sleep robot updates - Somnox blog [Internet]. 2021 [cited 2021 Aug 4]. Available from: https://meetsomnox.com/blog/somnox-sleep-robot-updates.
[10] Qoobo. Qoobo - A tailed cushion that heals your heart [Internet]. 2022 [cited 2022 Aug 4]. Available from: https://qoobo.info/index-en/.
[11] Jetpack Cognition Lab. Flatcat ~ your next robot is a pet. [Internet]. 2021 [cited 2021 Aug 4]. Available from: https://jetpack.cl/products/flatcat/.
[12] Furby Official Website. Furby boom, hasbro [Internet]. 2022 [cited 2022 Aug 4]. Available from: https://furby.hasbro.com/en-us.
[13] Moflin. Moflin is a totally new type of AI pet robot. [Internet]. 2021 [cited 4 Aug 2021]. Available from: https://www.moflin.com/.
[14] Makuake [Developed by Panasonic]. A free-spirited housemate robot "Nicobo" [Internet]. 2021 [cited 2023 Aug 4]. Available from: https://www.makuake.com/project/nicobo/.
[15] PARO. PARO Therapeutic robot [Internet]. 2021 [cited 2021 Aug 4]. Available from: http://www.parorobots.com/.
[16] Krishnan H, Vidyasagar M. Control of a single-link flexible beam using a Hankel-norm-based reduced order model. IEEE International Conference on Robotics and Automation; 1988 Apr 24-29; Philadelphia, USA. USA: IEEE; 1988. p. 9-14.
[17] CALCULIX. A three-dimensional structural finite element program [Internet]. 2023 [cited 2023 Aug 4]. Available from: http://www.calculix.de/.
[18] FreeCAD. Your own 3D parametric modeler [Internet]. 2023 [cited 2023 Aug 4]. Available from: https://www.freecadweb.org/.
[19] Infineon. TLE5009 E1000, Analog, GMR, SMD - Infineon Technologies [Internet]. 2021 [cited 2021 Aug 4]. Available from: https://www.infineon.com/cms/en/product/sensor/magnetic-sensors/magnetic-position-sensors/angle-sensors/tle5009-e1000/.
[20] Zile G, Dakal B, Haoyan L, Nishino T, Mitake H, Hasegawa S. Nuibot: motion control system and visual programming environment for string driven soft mechanism. The Proceedings of JSME annual Conference on Robotics and Mechatronics (Robomec). 2019;2019:1P2-G10.
[21] Texas Instruments Incorporated. DRV8833 data sheet, product information and support TI.com [Internet]. 2021 [cited 2021 Aug 4]. Available from: https://www.ti.com/product/DRV8833.

[22] White NM, Ash J, Wei Y, Akerman H. A planar respiration sensor based on a Capaciflector structure. IEEE Sens Lett. 2017;1(4):1-4.
[23] Infineon. CapSense® technology [Internet]. 2021 [cited 2021 Aug 4]. Available from: https://www.cypress.com/products/capsense-controllers.
[24] SparkFun Electronics. Conductive Fabric - 12"x13" MedTex180 - DEV-10055 [Internet]. 2021 [cited 2021 Aug 4]. Available from: https://www.sparkfun.com/products/retired/10055.
[25] Venkateshiah SB, Ioachimescu OC. Restless legs syndrome. Crit Care Clin. 2015;31(3):459-72.
[26] Flenady T, Dwyer T, Applegarth J. Accurate respiratory rates count: So should you!. Australas Emerg Nurs J. 2017;20(1):45-7.